Int. J. Electrochem. Sci., 12 **(2017)** 6729 – 6741, doi: 10.20964/2017.07.12

International Journal of ELECTROCHEMICAL SCIENCE
www.electrochemsci.org

Influence of the Immersion Time and Temperature on the Corrosion of API X52 Steel in an Aqueous Salt Medium

Mónica Corrales-Luna[1], *O Olivares-Xometl*[2,*], *Natalya V Likhanova*[3], *Raquel E. Hernández Ramírez*[4], *Irina V. Lijanova*[5], *P Arellanes-Lozada*[2], *Elsa Arce Estrada*[1]

[1] Instituto Politécnico Nacional, ESIQIE, Departamento de Metalurgia y Materiales, Av. Instituto Politécnico Nacional S/N, Col. Lindavista, México D.F. 07300, México.
[2] Benemérita Universidad Autónoma de Puebla, Facultad de Ingeniería Química, Av. San Claudio, Ciudad Universitaria. Col. San Manuel, Puebla, Pue. 72570, México.
[3] Instituto Mexicano del Petróleo, Gerencia de Ingeniería de Recuperación Adicional, Eje Central Lázaro Cárdenas No. 152, Col. San Bartolo Atepehuacán, México D.F. 07730, México.
[4] Tecnológico de Estudios Superiores de Coacalco, 16 de Septiembre 54, Col. Cabecera municipal, Coacalco de Berriozábal, 55700, Estado de México, México.
[5] Instituto Politécnico Nacional, CIITEC, Cerrada Cecati S/N, Colonia Santa Catarina, Azcapotzalco, México D.F. 02250, México.
[*]E-mail: oxoctavio@yahoo.com.mx

Received: 17 March 2017 / *Accepted:* 30 April 2017 / *Published:* 12 June 2017

Surface analyses aimed at assessing the corrosion damage suffered by API 5L X52 steel as a result of long immersion times in an aqueous salty medium (ASM), in absence and presence of oxygen, were carried out. The ASM chemical analyses revealed high concentrations of inorganic and organic ions, which evidenced a highly corrosive medium. The characterization of the corrosion products formed after 60 days exposing the steel sample to the ASM was performed by X-ray photoelectron spectroscopy (XPS), which confirmed the presence of different iron oxide faces. The modeling of electrochemical impedance spectroscopy (EIS) spectra showed that the electric charge transfer is a function of the temperature and immersion time used to expose the steel sample to the aqueous medium. Finally, the SEM/EDX analyses confirmed the combined presence of a not-compact film with corrosion products and salts on the surface, having as a result, an irregular and porous surface topography.

Keywords: Carbon steel; Corrosion behavior; EIS; XPS; SEM

1. INTRODUCTION

In most industrial facilities and processes, the use of steel is unavoidable due to its mechanical properties and the oil/gas industry is not an exception [1]. In this industry, the study of the corrosive medium is fundamental in order to propose more viable alternatives to reduce the extent of the

expensive damages caused by corrosion [2-4]. As for oil extraction, the reservoirs produce huge water volumes and the characteristics and physical properties of the produced water, known as congenital water, change considerably depending on the geographical location of the field, geological formations and type of extracted oil [5,6]. On the other hand, the crude oil/water ratio is not constant throughout the productive life of the reservoir and at advanced exploitation stages the reservoir salty water volume is higher than that of crude oil. This aqueous salty medium (ASM) is one of the main technical, environmental and economical problems associated with the oil and gas production [7,8]. In general, this ASM is composed of dispersed oil, dissolved organic compounds, production chemicals, heavy metals and natural radioactive minerals [9-11]. Due to the salty medium characteristics, the evaluation of the corrosion of carbon steel is of great interest for the industry because this phenomenon is responsible for high economical costs and human losses [8,12,13]. A specific case related to the aforementioned facts is the internal corrosion of carbon steel pipelines, which is a major problem that has caused numerous operation failures; in this sense, a frequently found damage type associated with salty media is the corrosion provoked by the formation of salt crusts in pipelines and heat transfer pieces of equipment, which affects seriously the overall efficiency of the extraction-transport-processing system. In addition, pitting corrosion damage caused by the high concentration of Cl^- and SO_4^{2-} ions is also commonly identified [14].

In addition, CO_2, sulfur-reducing bacteria (SRB), dissolved oxygen (DO), and hydrogen sulfide (H_2S) promote the corrosion of pipelines, which could turn into huge security risks [15-17]. Based on all the facts exposed above, the present work introduces a study of the damage suffered by API 5L X52 steel when exposed to an ASM in the presence and absence of oxygen. The EIS, XPS and SEM/EDX techniques were performed at different exposure days and temperatures.

2. EXPERIMENTAL

Table 1. Composition of the corrosive medium.

Physical properties		**Dissolved and suspension solids (mg/L)**	
Temperature (^{0}C)	25	Total dissolved solids	227,117.12
pH (a 25^{0}C)	4.82	Total hardness	98,944
Density (a 25^{0}C)	1.1017	Calcium/Magnesium hardness	41,193/57,751
Conductivity (μ/sm a 25^{0}C)	181,693	Alkalinity	637
Turbidity (FTU)	9	Salinity (NaCl)	288,000
Color (Pt-Co)	52	Stiff & Davis Stability Index	1.24
Cations (mg/L)		**Anions (mg/L)**	
Sodium (Na^+)	61,740.0	Chloride (Cl^-)	166,260.0
Calcium (Ca^{2+})	16,477.2	Sulfate (SO_4^{2-})	3.9
Magnesium (Mg^{2+})	14,033.5	Bicarbonate (HCO_3^-)	777.1
Iron (Fe^{2+})	19.9		
Total:	92,270.6	Total:	167,041.0

The ASM used to perform the electrochemical tests was obtained directly from a reservoir. The Stiff and Davis analysis data are shown in Table 1.

API 5L X52 steel with a contact area of 0.19 cm^2 was used. Prior to each test, the surface was polished with silicon carbide papers ranging from 240 to 2000 grades. Afterwards, the steel sample was washed with deionized water and acetone, subsequently submitted to an ultrasonic cleaning bath for 5 minutes in ethanol to be finally dried with N_2 flow. Electrochemical impedance spectroscopy (EIS) measurements were carried out using an AC signal with a potential of perturbation of 5 mV peak to peak with respect to OCP within a frequency interval from 100 kHz to 10 Hz and 50 steps. These tests were performed in a conventional cell for 32, 48, 64 and 80 days in absence and presence of oxygen in the studied medium at 25 and 45 °C. All the potentials are referred to a saturated calomel electrode (SCE) used as reference. The working electrode was API 5L X52 steel and the counter electrode was graphite. The piece of equipment and software used for these tests were an AUTOLAB potentiostat/galvanostat instrument model PGSTAT302N and NOVA 1.8, respectively. The XPS analyses were performed on a spectrometer equipped with a Kα X-ray source of 1486.6 eV. The analyzer energy was 23.5 eV at a base pressure of 4.5 X 10^{-8} Pa. The analyzed samples were immersed in the salty medium in presence and absence of oxygen for 60 days at 25 °C. The obtained spectra were adjusted to the C 1s (284.6 eV) peak. The chemical species were identified by fitting the spectrum curves using the Gaussian distribution, and a deconvolution procedure was employed to assign the high resolution spectra to the corresponding species. A scanning electron microscope (SEM) model SEM JEOL-JSM-6300 equipped with an energy dispersive spectrometry module at an accelerating voltage of 20.0 kV and magnification 1000x was used to obtain the corresponding steel sample micrographs.

3. RESULTS AND DISCUSSION

3.1 Characterization of the ASM

The Stiff and Davis analysis results are reported in Table 1, where it can be observed that the salty medium presents high concentrations of anions and cations in the next order: $Cl^- > HCO_3^- > SO_4^{2-}$ and $Na^+ > Ca^{2+}, Mg^{2+} > Fe^{2+}$. The physical and chemical properties as well as dissolved and suspension solids present in the aqueous medium support that it has corrosive properties.

3.2 Characterization of the steel surface by XPS

Table 2. Atomic percentages of the elements present on the API 5L X52 steel surface exposed to the ASM for 60 days at 25 °C.

	Atomic percentage (%)						
	C 1s	O 1s	Cl 2p	Fe 2p	Ca 2p	Na 1s	S 2p
Presence of O_2	30.4	27.5	23.7	8.1	7.8	2.5	0
Absence of O_2	34.55	21.87	27.58	3.81	9.68	2.23	0.29

Table 2 reports the elements found from the general spectrum (survey) performed on the steel surface exposed to the corrosive medium in the absence and presence of oxygen for 60 days. It can be seen that the intensity of the C 1s, O 1s, Cl 2p and Fe 2p is higher than the rest of the present elements. In different corrosive media, these elements are associated with the formation of corrosion products. The high chloride concentration is related to the formation of sodium chloride, calcium chloride and iron chloride. In addition, the amounts of iron and oxygen in the steel sample exposed to the corrosive medium in the absence of oxygen are lower. This result is due mainly to a lower formation of Fe^{3+} oxyhydroxides.

Figure 1 shows the Fe 2p high resolution spectrum, where the main doublet located at 708.9 eV (Fe $2p_3$) and 722.4 eV (Fe $2p_1$) with their corresponding satellite structures at 715 (Fe $2p_3$) and 728.8 (Fe $2p_1$) eV represent iron with oxidation state (II). Iron in the aggressive medium produces Fe(III) ions, which frequently in pH values close to neutrality form iron hydroxides ($Fe(OH)_2 \cdot nH_2O$), which by hydrolysis and/or oxidation effect(s) are transformed into "Green Rust" [18]. The shape and position of the peaks at 711.1 and 723.8 eV indicate the presence of oxyhydroxides, $Fe^{3+}(FeOOH)$, which can be represented by lepidocrocite, goethite, etc. In addition, it is possible to identify two types of iron salts such as iron chlorides at 710.3 and 729.0 eV and iron sulfates at 712.8 and 726.3 eV, which are formed at low concentrations on the surface. Finally, the peaks at 706.5 and 719.4 eV are characteristic of metallic iron (Fe^0).

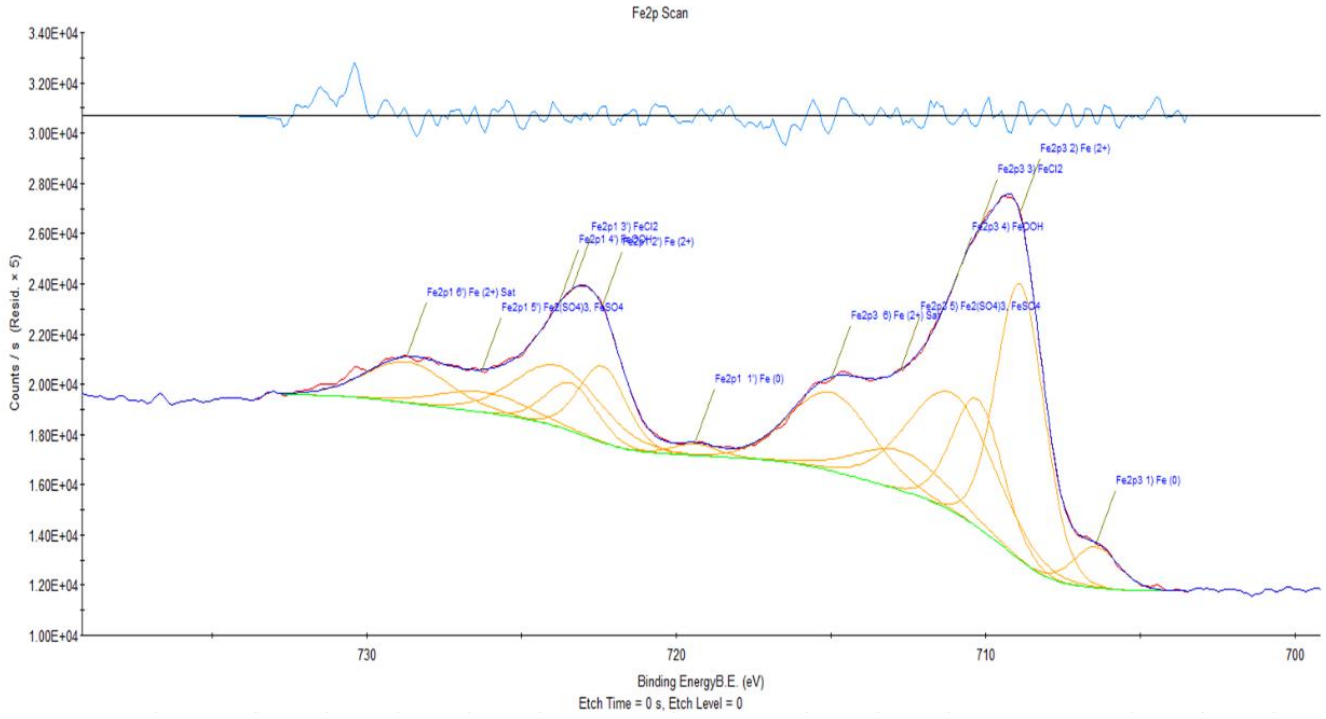

Figure 1. Fe 2p XPS spectrum of API 5L X52 steel exposed to the ASM for 60 days in the presence of oxygen.

Figure 2 corresponds to the Fe 2p high resolution spectrum of the steel sample exposed to ASM in the absence of oxygen. It can be observed that the species with higher concentration are the iron (III)

(711.1 and 723.8 eV) and iron (II) oxyhydroxides located at 708.8 eV (Fe $2p_3$) and 721.1 eV (Fe $2p_1$) with their corresponding satellite structures at 715 (Fe $2p_3$) and 728.4 (Fe $2p_1$) eV. It is also possible to distinguish two types of iron salts: iron chlorides at 710.1 and 722.4 eV and iron sulfates at 713.3 and 725.6 eV, which are formed at low concentrations on the surface. Finally, the peaks at 706.4 and 719.1 eV are characteristic of metallic iron (Fe^0).

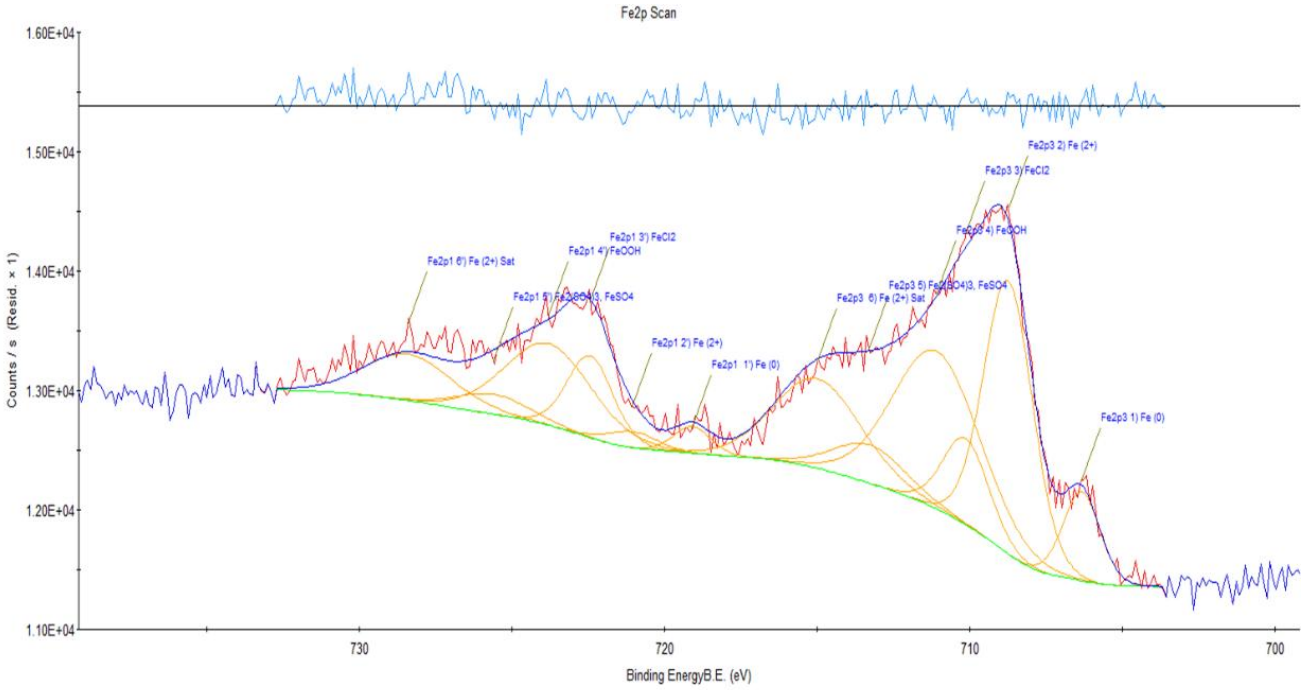

Figure 2. Fe 2p XPS spectrum of API 5L X52 steel exposed to the ASM for 60 days in the absence of oxygen.

3.3 EIS measurements

3.3.1 ASM in presence of oxygen

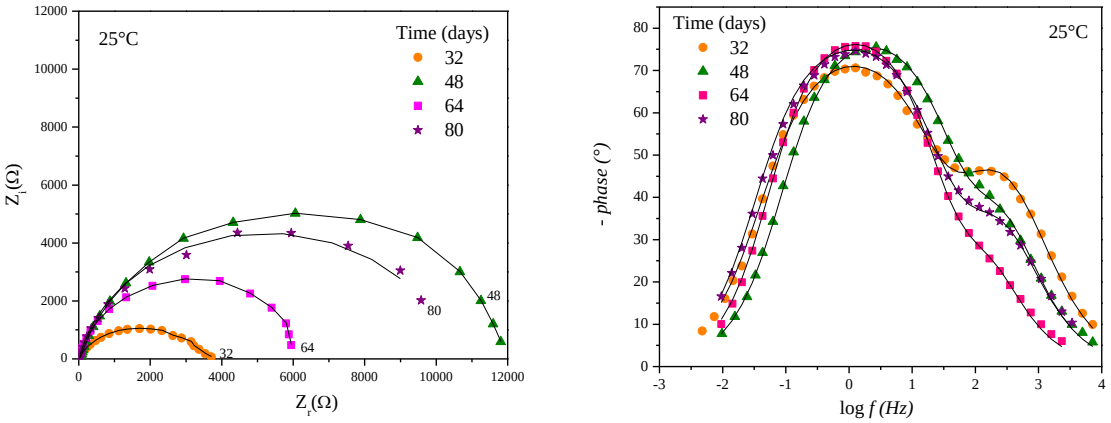

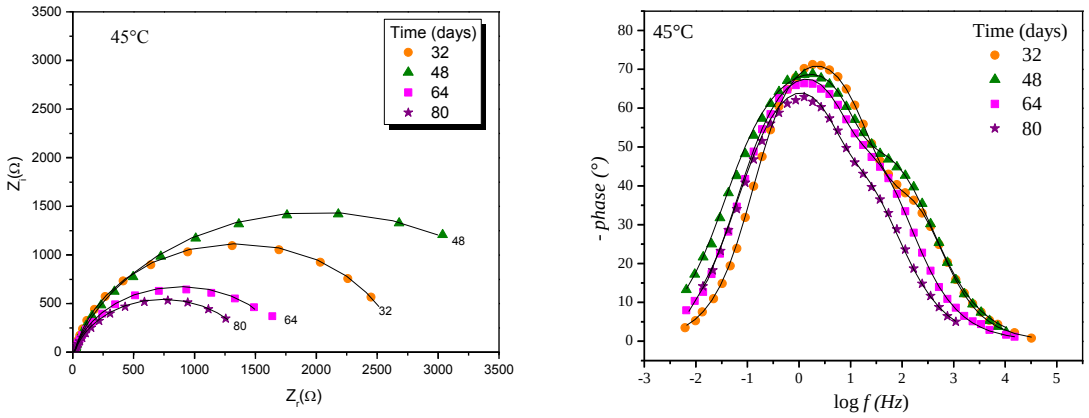

Figure 3. Nyquist and Bode plots of API 5L X52 steel in the ASM at 25 and 45 °C in the presence of oxygen.

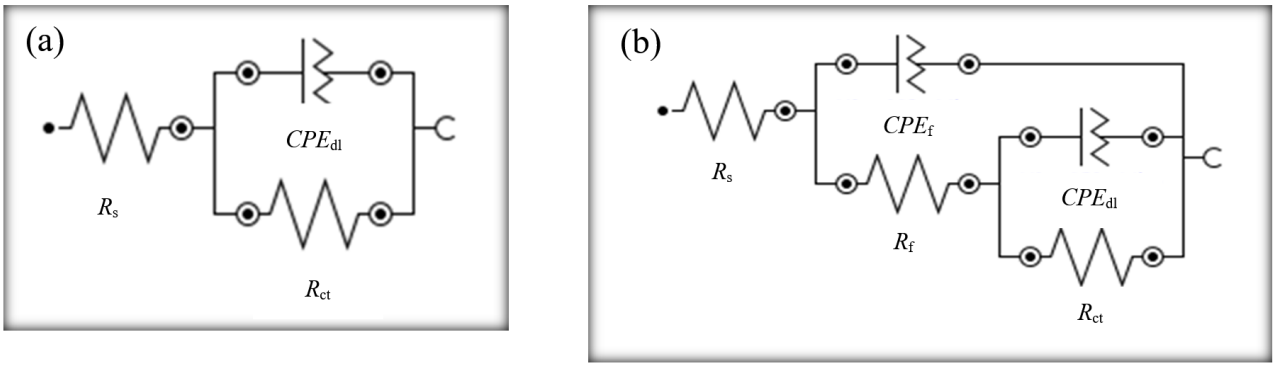

Figure 4. EC diagrams used to fit the EIS spectra in the ASM: (a) absence of oxygen at 45 ºC and (b) rest of the systems.

Figure 3 shows the Nyquist and Bode diagrams at 25 and 45 °C obtained from exposing the steel sample to the corrosive medium in the presence of oxygen, measured at different immersion times of 32, 48, 64 and 80 days, where changes are observed as a function of time. This fact indicates that the charge transfer and resistive processes occurring on the steel surface depend on the immersion time and affect directly the electric charge transfer in the interface phenomena [19]. The Nyquist diagrams are not perfect semicircles due to frequency dispersion [20,21] and show two overlapped capacitive loops, one at high frequency and the second at low frequency. The first capacitive loop represents the double layer capacitance of the electrode reaction [22,23], and the second capacitive loop at low frequency has been related to the fact that the sample surface was partially covered with corrosion products [24]. The Bode plots confirm that there are two time constants in the whole studied frequency range. The impedance spectra were fitted following the nonlinear least squares fitting (NLSF) procedure using an equivalent circuit (EC) in order to give a physical interpretation of the EIS spectra obtained in the present study. Figure 4 (b) shows the equivalent circuit (EC) used to fit the EIS data at 32, 48, 64 and 80 immersion days of API 5L X52 steel in the aqueous medium at 25 and 45 ^{o}C in presence of oxygen, where R_s is the solution resistance, CPE_f is the constant phase element related

to the adsorption process, R_f is the resistance of the film of corrosion products, CPE_{dl} is the constant phase element associated with the double layer capacity and R_{ct} is the charge transfer resistance.

The EC model used to describe metal–solution interface shows acceptable convergences between the experimental and theoretical fitted data if constant phase elements are involved in the EC. The impedance, *Z*, associated with the *CPE* element may be described as follows [25,26]:

$$Z_{CPE} = \left[Q\left(i\omega_{\max}\right)^{n} \right]^{-1} \quad (1)$$

where *Q* is the magnitude of *CPE* (Ω^{-1} s^n cm^{-2}), ω_{max} is the sine wave modulation angular frequency ($w = 2\pi f_{max}$, rad s^{-1}), *i* is the imaginary number and *n* is an exponent which determines the deviation from the ideal capacitive behavior [27,28]. In general, the use of a *CPE* is required for modelling the frequency dispersion behavior corresponding to different physical phenomena such as surface heterogeneity, which results from surface roughness, impurities, dislocations, grain boundaries, distribution of active sites and formation of porous layers [25]. Depending on the *n* value, the *CPE* can represent pure resistance (*n* = 0, *Q* = *R)*, pure capacitance *(n* = 1, *Q* = *C)*, pure inductance *(n* = -1, *Q* = *L)*, or Warburg impedance *(n < 1, Q = W).* In this context, *n* can be used as a measurement of surface faults [24]. Capacitance values were calculated using the following equation [28]:

$$C_{dl} = \left[Q_{dl} R_{ct}^{1-n_{dl}} \right]^{1/n_{dl}} \quad (2)$$

The values of the parameters obtained from fitting the EIS data by using EC are summarized in Table 3. It is evident that the EIS spectra do not feature a well-defined trend due to the changes regarding the charge transfer and resistive processes. The behavior of such spectra shows the instability and existence of a surface covered partially by corrosion products. It is observed that R_s is relatively constant between 32 and 80 days, but R_f values are affected by the time. The increase of R_f values are correlated with the pseudo-passivation. The decrease and increase of R_{ct} evidence the adsorption and desorption of corrosion products such as FeOOH, Fe_xO_y and $Fe(OH)_2$ on the steel surface, affecting the charge transfer process of the steel sample. As the system does not feature an ideal behavior, *n* values are related to the formation of a porous film of corrosion products with irregular topography, which is confirmed by XPS and SEM.

Table 3. Parameters obtained by fitting EIS data to the EC for the API 5L X52 steel system at 25 and 45 °C in the presence of oxygen in the ASM.

Temperature (°C)	**Immersion Time** (Day)	R_s (Ohm cm^2)	C_f (μFcm^{-2})	n_1	R_f (Ohm cm^2)	C_{dl} (μFcm^{-2})	n_2	R_{ct} (Ohm cm^2)
25	32	6.87	18.79	0.82	24.77	157.60	0.68	3654
	48	7.41	41.04	0.82	82.34	165.60	0.87	12364
	64	6.94	62.87	0.87	30.58	148.10	0.91	6257
	80	7.68	61.68	0.84	31.95	239.30	0.90	10407
45	32	7.28	93.91	0.85	31.72	226.30	0.90	2655
	48	4.67	193.20	0.80	41.93	313.30	0.84	1828
	64	4.66	192.93	0.80	41.23	360.40	0.83	3972
	80	8.71	172.25	0.71	98.80	350.00	0.95	1380

The increase in n_2 values could be due to two factors: a) the lack of adsorption-desorption equilibrium and the surface heterogeneity, and b) the ohmic current drop [26]. The behavior of C_{dl} indicates a strong influence of the surface conditions and the chemical properties close to the surface, and because of this fact, it was related to the double layer information and the adsorbed corrosion products [29]. The R_{ct} decrease and increase as time passes, this could be by is due to the adsorption-desorption of the corrosion products and salt layers deposited on the surface according to the XPS/SEM analysis. The immersion time due to the temperature accelerates the dissolution velocity and the formation of the layer of corrosion products [30]. Therefore, such a film has to be physically dense and porous (SEM), which helps the ions diffusion (Cl^-, OH^- and SO_4^{2-}) in the metal-oxide interface; as a consequence, the mass loss suffered by the steel sample is unavoidable; this behavior is supported by the *n* data.

3.3.2 ASM in absence of oxygen

Figure 5 shows the EIS spectra obtained for API 5L X52 steel immersed in an ASM in the absence of oxygen at 25 and 45 °C. It can be observed that Z_r and Z_i do not feature a well-defined trend due to the instability and existence of a surface covered partially by corrosion products.

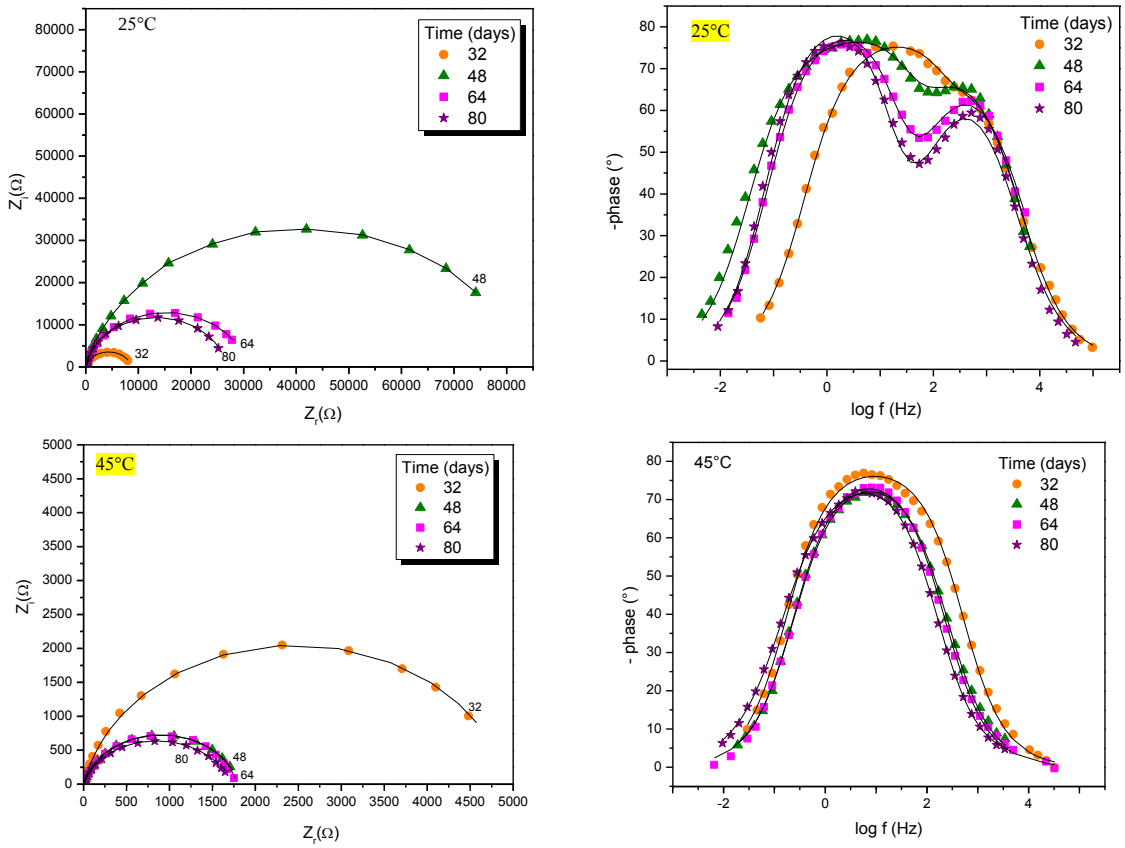

Figure 5. Nyquist and Bode plots of API 5L X52 steel in the ASM at 25 and 45 °C in the absence of oxygen.

The film of corrosion products allows the ions diffusion (Cl^-, OH^-, SO_4^{2-} etc.) and favors the steel oxidation. Studies performed using different corrosive media in the presence of oxygen have reported that these elements favor a higher corrosion velocity due to the combination between oxygen-iron ions [31,32]. In the present work, such a result was also obtained according to the behavior shown in Figure 5.

It can be stated that the steel corrosion in the absence of oxygen is controlled anodically by the formation of a non-passive $FeCl_2$ film and NaCl and carbonate precipitates (XPS). In the case of the Fe_xCl_y precipitate, which is formed in the anodic reaction, tends to be hydrolyzed, freeing once again the Cl^- ions, which originate a cyclic reaction process with the formation of Fe_xCl_y and NaCl with time. These products deposited on the surface affect the Z_r vs Z_i response.

Table 4 reports the data obtained from fitting the spectra featured in Figure 5 corresponding to 25 and 45 ^oC, respectively. It can be observed that at 25 ^oC, R_s is increased whereas C_f shows a trend to be diminished, both as functions of time, while the n data are below the unit. The R_{ct} data do not present a well-defined trend due to the constant change in the interface of metal-corrosion products caused by the dissolution of the corrosion products or/and diffusion of ions that affect the double electric layer. Nevertheless, these surface changes make possible the presence of damage by "pitting" localized corrosion caused by the high concentrations of Cl^- ions according to the studies reported about saline media [33].

Table 4. Parameters obtained by fitting EIS data to the EC for the API 5L X52 steel system at 25 and 45 °C in the absence of oxygen in the ASM.

Temperature (°C)	**Immersion Time** (Day)	R_s (Ohm cm^2)	C_f (μFcm^{-2})	n_1	R_f (Ohm cm^2)	C_{dl} (μFcm^{-2})	n_2	R_{ct} (Ohm cm^2)
25	32	3.53	8.50	0.85	190.64	1.06	0.70	8543
	48	5.09	7.87	0.83	550.30	4.71	0.70	82381
	64	5.12	6.23	0.89	177.60	44.04	0.91	30008
	80	6.08	6.09	0.89	153.18	65.08	0.93	26516
45	32	4.37	182.70	0.88	4929	-	-	-
	48	4.45	348.07	0.86	1801	-	-	-
	64	4.58	377.10	0.87	1781	-	-	-
	80	4.08	437.23	0.81	1723	-	-	-

The shown behavior patterns are similar for both temperatures, however, at 45 °C, only one time constant is present and the EC used was that of Figure 4 (a). The diffusion process of ions in the metal-solution interface occurs faster because of the temperature effect. This fact helps suppose that during the development of the redox reaction, the formation of salts and Fe_xCl_y occurs due to the fact that their concentrations do not change in the medium, notwithstanding, their formation and dissolution velocity is higher due to the temperature increase. Thus, the formation of such a film has to be based

on the equilibrium between the salts and medium, where the equilibrium factors are the chloride, sulfate and carbonate ions in the corrosive medium. The C_{dl} data do not show a constant behavior.

In general, in both studies, the results confirm constant changes occurring on the steel surface exposed to the studied medium. The formation of the different corrosion products and salts confirmed by XPS affects the metal-corrosion products interface, which in turn affect the velocity of the electric charge transfer in the double layer. In addition, these processes are affected by the morphology changes suffered by the films: instability, roughness, thickness and chemical composition.

3.4 Surface analysis by SEM/EDX

Figures 6 and 7 show the API 5L X5 steel surface after 16 days of immersion in an ASM in the presence of oxygen at 25 and 45 °C. Both figures show the formation of corrosion products on the surface, which are mainly different faces of iron oxides (XPS), and salts (NaCl, Mg_2Cl, Ca_2Cl, etc.), according to the signals of the elements obtained by the EDX analysis. Figures 3 and 5 (EIS) and the micrographs in Figures 6 and 7 support the *n* data obtained by means of the EIS modeling with the EC. The presence of a corrosion products layer with irregular topography, cracked and porous, is confirmed. These layer characteristics affect the diffusion processes of the aggressive ions according to the R_{ct} data obtained as functions of the immersion time and temperature.

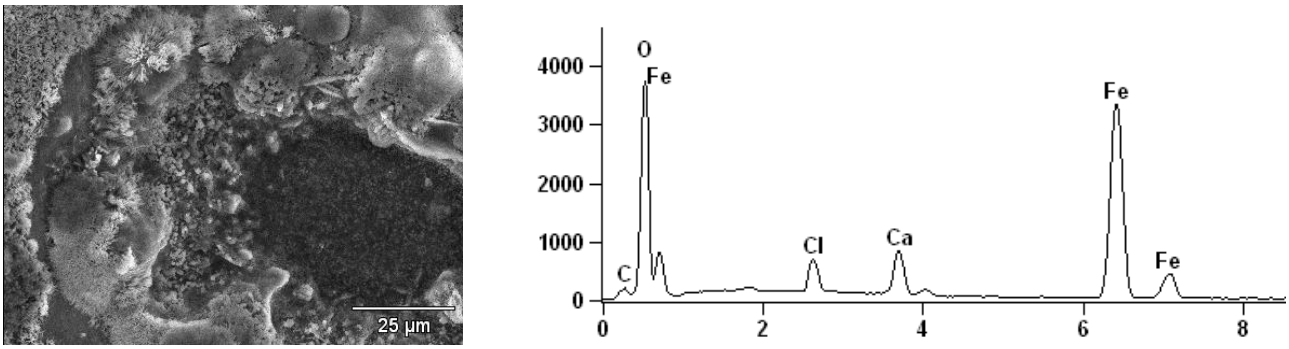

Figure 6. Micrograph (1000 X) of the API 5L X52 steel surface exposed to the ASM in the presence of oxygen at 16 days and 25 °C.

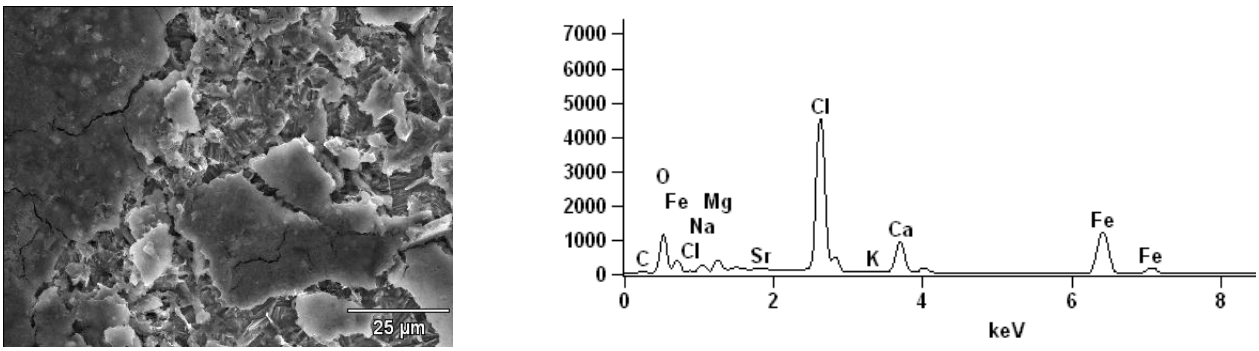

Figure 7. Micrograph (1000 X) of the API 5L X52 steel surface exposed to the ASM in the presence of oxygen at 16 days and 45 °C.

Likewise, Figures 8 and 9 show a dense layer of corrosion products formed by the oxidation reaction after 64 days at 25 and 45 ^{o}C. The high intensity of the chlorine and calcium elements (EDX) indicates the presence of salts in combination with the layer of oxides. This layer, which was formed similarly, features characteristics that are similar to those observed previously, however, due to the medium characteristics, the presence of zsomolnokite, goethite, lepidocrocite, ferrihydrite, and FeOOH, among others, is possible [30,34]. The characteristics shown in Figures 8 and 9 support the discussion about the EIS spectra and the data obtained from the ECs (Figure 4). Notwithstanding, according to all the obtained results, it is important to point out that the studied ASM is corrosive even in the absence of oxygen due to the high concentrations of ions that it has.

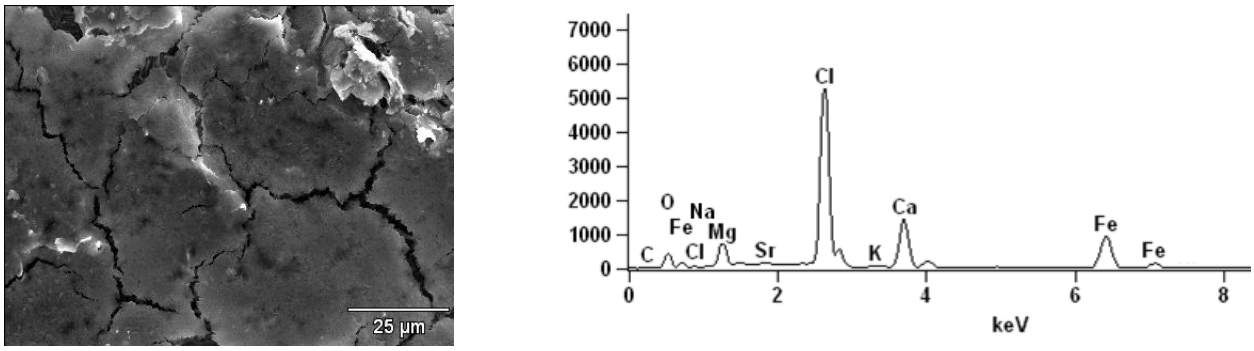

Figure 8. Micrograph (1000 X) of the API 5L X52 steel surface exposed to the ASM in the absence of oxygen at 64 days and 25 °C.

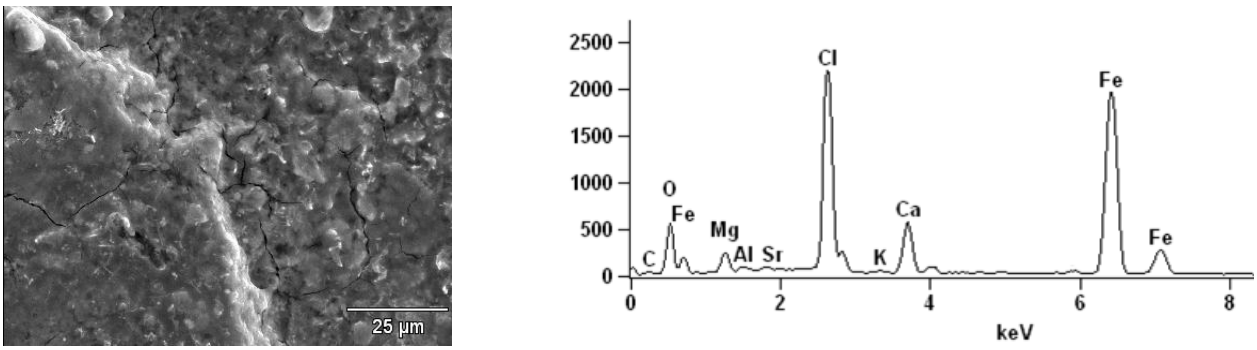

Figure 9. Micrograph (1000 X) of the API 5L X52 steel surface exposed to the ASM in the absence of oxygen at 64 days and 45 °C.

4. CONCLUSIONS

The high concentrations of Cl^-, SO_4^{2-} and HCO_3^- ions in the ASM make of it a highly corrosive one, where the presence/absence of oxygen does not reduce the medium aggressiveness.

The XPS technique helped establish that the chloride ions and water molecules were adsorbed firstly on the metal surface forming $(OH)_2 \cdot nH_2O$ and $Fe(OH)Cl \cdot n(H_2O)$ complexes and iron

oxyhydroxides $(FeOOH)$ of the lepidocrocite $[\gamma\text{-}FeO(OH)]$, goethite $[\alpha\text{-}FeO(OH)]$, ferrihydrite $\left[\left(Fe^{3+}\right)_2 O_3 \cdot 5H_2O\right]$ and zsomolnokite $FeSO_4 \cdot H_2O$ types.

The EIS analysis showed significant differences in the magnitudes of the spectra, which depended on the immersion time of the steel sample in the salty medium and the temperature. In all the analyses, it was observed that the velocity of the electric charge transfer in the double layer is affected by the corrosion products.

The SEM analysis confirmed the formation of porous films of corrosion products in all the cases with irregular topographies caused by the presence of different iron oxide faces. According to the aforementioned, the corrosion process suffered by the steel sample was always dynamic without passivation stages.

ACKNOWLEDGEMENTS
The authors gratefully acknowledge Conacyt-México and SNI for the scholarship provided and appreciate the support given by BUEP-VIEP and ESIQIE-IPN.

References

1. H. Liu, T. Gu, G. Zhang, W. Wang, S. Dong, Y. Cheng and H. Liu, *Corros. Sci.*, 105 (2016) 149.
2. L. Fragoza Mar, O. Olivares-Xometl, M. A. Dominguez-Aguilar, E. A. Flores, P. Arellanes-Lozada and F. Jiménez Cruz, *Corros. Sci.*, 61(2012) 171.
3. M. E. Belghiti, Y. Karzazi, A. Dafali, I. B. Obot, E. E. Ebenso, K. M. Emran, I. Bahadur, B. Hammouti and F. Bentiss, *J. Mol. Liquids*, 216 (2016) 874.
4. C. Verma and M. A. Quraishi, *Anal. Bioanal. Electrochem*., 8 (2016)104.
5. H. R. A. Hamid, W. M. S. Kassim, A. El Hishir and S. A. S. El-Jawashi, *Environ. Monit. Assess*, 145 (2008) 95.
6. S. E. Weschenfelder, A. M. T. Louvisse, C. P. Borges, E. Meabe, J. Izquierdo and J. C. Campos, *J. Petrol. Sci. Eng.*, 131 (2015) 51.
7. X. Wang and R. E. Melchers, *J. Loss. Prevent. Proc*., 45 (2017) 29.
8. R. Hosny, M. Fathy, M. Ramzi, Th. Abdel Moghny, S. E. M. Desouky and S. A. Shama, *Egypt. J. Petrol.*, 25 (2016) 391.
9. S. S. M. Tavares, J. M. Pardal, F. B. Mainier, H. R. da Igreja, E. S. Barbosa, C. R. Rodrigues, C. Barbosa and J. P. Pardal, Eng. *Failure Analysis*, 61 (2016) 100.
10. A. Alkhudhiri, N. Darwish and N. Hilal, *Desalination*, 309 (2013) 46.
11. B. Dong, Y. Xu, S. Jiang, and X. Dai, *Desalination*, 372 (2015) 17.
12. L. Torres, O. P. Yadav and E. Khan, *Sci. Total Environ*., 529 (2016) 478.
13. J. Lee, S. Han, K. Kim, H. Kim and U. Lee, *Eng. Fail. Anal*., 34 (2013) 300.
14. G. Li, S. Guo, J. Zhang and Y. Liu, *Desalination*, 351(2014) 213.
15. G. A. Zhang and Y. F. Cheng, *Corros. Sci*., 52 (2010) 2716.
16. Z. D. Cui, S. L. Wu, S. L. Zhu and X. J. Yang, *Appl. Surf. Sci*., 252 (2006) 2368.
17. Y. Liu, Y. Zhang and J. Yuan, *Eng. Failure Analysis*, 45 (2014) 225.
18. H. Sakurai, J. Tamura and T. Yoshimura, *Inorg. Chem*., 24 (1985) 4363.
19. F. Bentiss, M. Lebrini, H. Vezin, F. Chai, M. Traisnel and M. Lagrené. *Corros. Sci*., 51 (2009) 2165.
20. M. A. Deyab, S. T. Keera and S. M. El Sabagh. *Corros. Sci.*, 53 (2011) 2592.

21. Q. Cheng and Z. Chen, *Int. J. Electrochem. Sci*., 8 (2013) 8282.
22. I. Zeng, G.A. Zhang and X.P. Guo, *Corros. Sci.*, 85 (2014) 318.
23. W. Liu, J. Dou, S. Lu, P. Zhang and Q. Zhao, *Appl. Surf. Sci*., 367 (2016) 438.
24. M. Keddom, O.R. Mattos and H. Takenouri, *J. Electrochem. Soc*., 128 (1981) 257.
25. P. B. Raja, A. K. Qureshi, A. Abdul Rahim, H. Osman and K. Awang, *Corros. Sci*., 69 (2013) 292.
26. K. C. Emregül and O. Atakol, *Mater. Chem. Phys*., 83 (2004) 373.
27. D. A. López, S. N. Simison and S. R. De Sánchez, *Electrochim. Acta*, 48 (2003) 845.
28. A. Popova, M. Christov and A. Vasilev, *Corros. Sci.*, 49 (2007) 3290.
29. F. B. Growcock and J. H. Jasinki, *J. Electrochem. Soc*., 136 (1989) 2310.
30. O. Olivares-Xometl, N.V. Likhanova, N. Nava, A. C. Prieto, I.V. Lijanova, A. Escobedo-Morales and C. López-Aguilar, *Int. J. Electrochem. Sci*., 8 (2013) 735.
31. Y.P. Kim, M. Fregonese, H. Mazille, D. Feron and G. Santarini, *Corros. Sci*., 48 (2006) 3945.
32. E. Zhuravlyova, L. Iglesias-Rubianes, A. Pakes, P. Skeldon, G. E. Thompson, X. Zhou, T. Quance, M. J. Graham, H. Habazaki and K. Shimizu, *Corros. Sci.*, 44 (2002) 2153.
33. A. M. Abdel-Gaber, B. A. Abd-El-Nabey, E. Khamis and D.E. Abd-El-Khalek, *Desalination*, 278 (2011) 337.
34. N. V. Likhanova, M. A. Domínguez-Aguilar, O. Olivares-Xometl, N. Nava-Entzana, E. Arce, H. Dorantes, *Corros. Sci.*, 52 (2010) 2088.